Unique Structure and Dynamics of Poly(ethylene oxide) in Layered Silicate Nanocomposites: Accelerated Segmental Mobility Revealed by Simulating ESR Spectra of Spin-Labels, XRD, FTIR, and DSC

Yohei Miwa,[†,§] Andrew R. Drews,[‡] and Shulamith Schlick*[,†]

Department of Chemistry and Biochemistry, University of Detroit Mercy, 4001 West McNichols Road, Detroit, Michigan 48221-3038, and Ford Research and Innovation Center, Ford Motor Company, MD 3179, P.O. Box 2053, Dearborn, Michigan 48121

Received January 29, 2008; Revised Manuscript Received May 12, 2008

ABSTRACT: The structure and dynamics of poly(ethylene oxide) (PEO) intercalated in the galleries of a fluoromica inorganic clay were studied by spin-label electron spin resonance (ESR), XRD, FTIR, and DSC. The polymer was end-labeled by attachment of a nitroxide radical. Basic structural information was determined by XRD, while DSC and FTIR revealed that the crystallization of the PEO was inhibited in the clay galleries. The temperature variation of the ESR spectra from the spin-label was simulated based on the "macroscopic order with microscopic disorder" (MOMD) model. For PEO intercalated in the narrow (0.33 nm) clay galleries, the ESR spectra indicated a very low segmental mobility even at high temperature, 410 K, which was attributed to the strong polymer interaction with the charged mica platelets. In wider (0.83 nm) galleries, however, the parameters used to simulate the ESR spectra of the nitroxide labels reflected a lowering of the PEO segmental density: In this sample, the ESR spectrum consisted of two distinct contributions from slow- and fast-motional components, and the relative intensity of the fast component increased with an increase in temperature. The two spectral components were attributed to segments located close to, and away from, the polar solid walls in the gallery, respectively. Interestingly, the fast-motional component had *higher* mobility compared to that of PEO chains adsorbed on the fluoromica surface. In addition, the activation energy of the segmental motion in the fast-motional component was *lower* compared to that of bulk PEO. The low segmental density and reduced cooperative motion with neighboring segments are considered the main factors leading to the fast PEO chain motion with low activation energy.

Introduction

Nanocomposites consisting of polymers intercalated in layered inorganic compounds have attracted great interest in recent years, both as novel materials with enhanced properties and as ideal systems for the study of polymer behavior in nanoscopically confined media.[1,2] In particular, poly(ethylene oxide) (PEO)/clay nanocomposites have been widely studied because of their unique electronic, ionic (without counterions), structural, thermal, and mechanical properties.[3–12] In these systems the PEO chains are confined in narrow, <1 nm wide, galleries between the inorganic layers.[3,4] The conformation and mobility of clay-intercalated PEO chains are expected to be quite different compared to bulk PEO; indeed, interesting results on intercalated PEO have been reported.[3–9,11] The polymer conformation and mobility in the PEO/clay nanocomposites are affected by the limited space and by the interaction with the charged surface of the inorganic host layers and interlayer cations, such as Na^+ or Li^+.[3,4,6,7,9–11]

The conformation of PEO intercalated in clay galleries has been the subject of several important papers. Aranda and Ruiz-Hitzky first proposed a helical conformation of the intercalated PEO, based on FTIR as well as ^{23}Na and ^{13}C solid-state NMR.[3] Harris et al. studied the conformation of intercalated PEO by double-quantum ^{13}C solid-state NMR; the results indicated a high gauche content (≈90%) of the OC−CO bonds.[9] The low trans content showed that long helical sections are not present. On the other hand, single or double all-trans PEO conformations due to adsorption of polymer layers on the inorganic host surfaces were suggested by Wu and Lerner.[4] However, Bujdák et al. claimed that the highly ordered structure is improbable on the basis of energetic considerations.[10] Recently, Giannelis and co-workers proposed disordered and liquidlike structure of PEO on the basis of computer simulations, ^7Li, ^{23}Na, and ^2H solid-state NMR, and X-ray diffraction and suggested that the cations are not interacting with the polymer chains.[5,6,11,13]

The dynamics of PEO intercalated in clay galleries has been studied by several techniques: solid-state NMR, thermally stimulated current (TSC), and dielectric spectroscopy.[6,8,14,15] Differential scanning calorimetry (DSC) showed no melting and glass transitions for PEO intercalated in clay nanocomposites. TSC data showed a broad relaxation starting at about the PEO glass transition temperature (T_g = 218 K) up to ≈333 K; the relaxation was characterized by a very low activation energy, E_a.[8] On the basis of this result, the authors proposed that the segmental relaxation of the PEO extended toward the higher temperature due to the constraining effect of the narrow gallery on some polymer conformations; moreover, E_a can decrease because the confinement reduced the cooperativity with neighboring segments.

The ^2H NMR line shapes of intercalated deuterated PEO (*d*-PEO) suggested two differences compared to bulk PEO: evidence for enhanced chain mobility from the appearance of the central peak at a lower temperature (250 K) compared to bulk PEO (270 K) and the presence of two spectral components, fast and slow, at 340 K only in the nanocomposite; bulk *d*-PEO showed only the fast relaxing component. This latter result indicated that the mobility of some conformations in intercalated PEO was low even at the high temperature.

Using dielectric spectroscopy, Elmahdy et al. found that the segmental dynamics of PEO intercalated in clay galleries was accelerated and followed an Arrhenius temperature dependence

* Corresponding author. E-mail: schlicks@udmercy.edu.
† University of Detroit Mercy.
‡ Ford Motor Company.
§ Present address: Mitsubishi Chemical Group Science and Technology Research Center, Inc., Japan.

10.1021/ma800214q CCC: $40.75
Published on Web 06/13/2008

Chart 1. Spin-Labeled PEO Chain

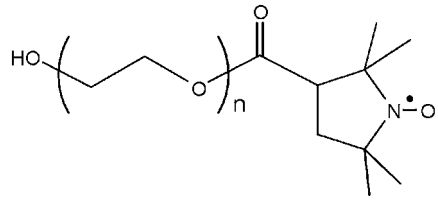

with a single activation energy, while the segmental relaxation of bulk PEO was better explained with two activation energies based on the Vogel−Fulcher−Tammann equation.[14,15] They concluded that the accelerated segmental dynamics was due to the inhibition of cooperative motions between neighboring segments in the confined space of the clay galleries. A fast relaxation process was also observed in the intercalated nanocomposites with poly(methylphenylsiloxane) confined within the 1.5−2.0 nm galleries of organically modified silicates.[16]

Electron spin resonance (ESR) based on spin-label and spin-probe techniques is a powerful method to discern different sites in complex systems and can provide detailed information on the local environment and dynamics on time scales in the range $10^{-11}-10^{-7}$ s. This approach has been applied to polymer/inorganic nanocomposites:[17–19] Brik et al. reported the first spin-label study, on PEO/silica nanocomposites synthesized via the sol−gel reaction, and reported that the polymer motion was hindered in the vicinity of the silica "nodes", a result that was verified by ^{13}C NMR.[17] Jeschke and his group studied the dynamics of a spin-labeled surfactant in organically modified silicates and their composites with polystyrene using CW and pulsed ESR techniques as well as ^{31}P MAS NMR.[18] Recently, we reported on the direct effect of the clay on polymer dynamics in a spin-label study of exfoliated poly(methyl acrylate) (PMA)/synthetic fluoromica (Somasif) nanocomposites.[19] The dynamics of PMA in the nanocomposite was studied, with focus on the interfacial region between Somasif and the PMA phase; the data suggested constrained mobility of the polymer at the interface and led to an estimate of the thickness of the rigid interface.

Here we present an ESR spin-label study of PEO intercalated and confined in the nanoscopic galleries between silicate platelets. The motivation for this study was to reveal the relationship between the gallery width and the segmental mobility of polymer chains embedded between inorganic walls. This study resulted in the first direct and quantitative analysis of the dynamics of the polymer chains confined in the clay galleries. The experimental results clearly indicated that the segmental mobility of the PEO was dependent on the gallery width. The detailed motional properties of intercalated PEO chains in terms of activation energy, correlation time, and local interactions were estimated from simulations of experimental ESR spectra. As described below, an interesting result was the detection of enhanced mobility of PEO segments in clay galleries of width 0.83 nm, which, we suggest, is due to the reduced segmental density, less entanglements, and lack of dynamic cooperativity of confined chains.

Experimental Section

Materials. Poly(ethylene oxide) having a number-average molecular weight $M_n = 4 \times 10^3$ (PEO4k) was purchased from Fluka Chemical Co., Ltd. Anhydrous pyridine (99.8%), thionyl chloride (≥99%), 3-(carboxy)-2,2,5,5-tetramethyl-1-pyrrolidinyloxy (3-carboxy-PROXYL), 4-hydroxy-2,2,6,6-tetramethylpiperidine 1-oxyl (TEMPOL), deionized water (CHROMASOLV), anhydrous diethyl ether (≥99.4%), toluene (≥99.5%), and hexanes (99.9%) were purchased from Aldrich and used as received. Benzene (≥99.5%, Aldrich) was dried with molecular sieves (8−12 mesh, beads effective pore size 10 Å, Fisher Scientific Co.) and calcium hydride (Eastman Kodak Co.).

Table 1. Characteristics of Samples

sample	Somasif/wt %[a]	$d_{gallery}$/nm[b]	T_m/K[c]
PEO4k			338
NANO96	96	0.33	
NANO82	82	0.83	
COMP99.8	99.8		

[a] Determined by TGA. [b] The gallery width in which PEO chains were intercalated (estimated from XRD data). [c] Determined by DSC.

Synthetic fluoromica (Somasif ME-100) was supplied by CO-OP Chemical Co., Ltd., Japan. The chemical composition and the cationic exchange capacity of Somasif were $Na_{0.66}Mg_{2.68}(Si_{3.98}Al_{0.02})O_{10.02}F_{1.96}$ and 115 mequiv/g, respectively.[20]

Synthesis of Spin-Labeled PEO4k. PEO4k was purified by precipitation from benzene solution to diethyl ether and dried at 343 K in vacuum for 24 h. This procedure was repeated twice. The chain end of the PEO was spin-labeled as shown in (Chart 1) by the method of Törmälä and Lindlberg.[21] A solution of thionyl chloride (0.06 mL) in dry benzene (2 mL) was added dropwise to a solution of 3-carboxy-PROXYL (0.05 g) in a mixture of dry benzene (8 mL) and pyridine (0.07 mL) while stirring. The reaction mixture was next stirred at 283 K for 1 h and at room temperature for 2 h and added dropwise while stirring to a solution of PEO (15 g) in a mixture of dry benzene (100 mL) and pyridine (0.04 mL). The reaction mixture was then stirred at 283 K for 5 h and overnight at room temperature. Pyridine hydrochloride was removed by filtration. The spin-labeled PEO4k was purified by precipitation from a benzene solution to diethyl ether. After precipitation, the resulting sample was dried at 318 K in vacuum for 18 h, a process that was repeated four times. The ESR signal of the solution was measured; after the fourth precipitation, no ESR signal was detected, indicating complete removal of unreacted 3-carboxy-PROXYL. Both chain ends of PEO chains may become spin-labeled, but the distance between the labels is large enough to avoid spin exchange. Moreover, spin-labeled PEO was admixed with nonlabeled PEO at 348 K in order to avoid a high concentration of the spin-label. The concentration of the spin-labels in the PEO mixture was determined to be $\approx 1 \times 10^{-6}$ mol/g, using a standard solution of TEMPOL in toluene as an intensity reference.

Preparation of PEO/Somasif Nanocomposites. The notation used for the composites is NANO*m* for intercalated nanocomposites and COMP*m* for nonintercalated composites, where *m* is the Somasif wt %; the *m* values in the NANO*m* series were determined by TGA measurement. The characteristics of the samples used in this work are listed in Table 1. NANO82 was prepared via a melt intercalation method following Wong et al.[6] For lower PEO content, we could not obtain a nanocomposite with ordering intercalated structure, as the XRD pattern of this sample showed no distinct diffraction peaks from intercalated layers (see Supporting Information). Therefore, NANO96 was prepared via the solution intercalation method.[4]

Melt Intercalation Method. Somasif and PEO powders were mixed and pressed into a pellet and annealed at 353 K in vacuum for 12 h. The resulting pellet was ground and pressed again into a pellet and reannealed under similar conditions until no melting point was observed by DSC. Finally, the nanocomposite was ground to a fine powder, washed with benzene to remove the nonintercalated polymer completely, and dried in a vacuum oven at 353 K for 24 h.

Solution Intercalation Method. Somasif was dispersed in deionized water to a concentration of 1.5 wt %. The dispersion was ultrasonicated and stirred until a homogeneous system was observed, usually for 1−3 h. The spin-labeled PEO was dissolved in water to a concentration of 1.5 wt %. This solution was added dropwise to the Somasif dispersion, and the mixture was vigorously stirred for 6 h, followed by solvent evaporation. The sample was then dried in a vacuum oven at 333 K for 6 h. Next, the dried sample was powdered using a mortar and pestle, dried again at 333 K for 24 h, and washed with benzene to remove the

nonintercalated PEO. The nanocomposite was finally dried in a vacuum oven at 353 K for 24 h.

Preparation of PEO/Somasif Nonintercalated Composites. Spin-labeled PEO was dissolved in benzene to a concentration of 1 wt %. The PEO solution was poured into a Somasif/benzene dispersion with a concentration of 5 wt %. Benzene was evaporated while stirring in a hood. The remaining powder was dried at room temperature in vacuum for 24 h. It should be noted that PEO in COMP99.8 was easily flushed with benzene, while PEO in both NANO96 and NANO82 was not flushed.

ESR Measurements. ESR samples were prepared by loading powders into 4 mm o.d. quartz tubes and heated under vacuum to remove adsorbed water before sealing (PEO4k and COMP99.8 were heated to 353 K; NANO96 and NANO82 were heated to 373 K). Spectra were recorded with Bruker X-band EMX spectrometers operating at 9.7 GHz with 100 kHz magnetic field modulation and equipped with the Acquisit 32 Bit WINEPR data system version 3.01 for acquisition and manipulation, and the ER4111VT variable temperature unit. The microwave frequency was measured with a Hewlett-Packard 5350B microwave frequency counter. Most spectra were collected with the following parameters: sweep width 120 G, microwave power 2 mW, time constant 20.48 ms, conversion time 40.96 ms, 2−16 scans, and 2048 points. The modulation amplitude was varied in the range 0.5−3 G, depending on the line width. The temperature was controlled within ±1 K. All samples were allowed to equilibrate for at least 15 min after reaching the desired temperature.

Simulation of ESR Spectra. ESR spectra were calculated with the software based on the stochastic Liouville equation.[22] Simulated spectra were fitted to experimental spectra using a PC version of the NLSL program based on the modified Levenberg−Marquart minimization algorithm, which iterates the simulations until a minimum least-squares fit to experiment is reached.[23] The g and ^{14}N hyperfine tensors were determined by analyzing rigid-limit spectra measured at 100 K.

The model known as "microscopic order with macroscopic disorder" (MOMD) was applied for calculating the spin-label rotational diffusion.[24] The model assumes that the spin-labels undergo microscopic molecular ordering with respect to a local director; the local directors in the sample are randomly oriented in the laboratory frame. Pilar summarized recently the successful application of the MOMD model for analyzing ESR line shapes of spin-labeled polymers.[25] When applied to spin-labels attached to polymers via short tethers, the MOMD model implies a preferred orientation for the axis of internal rotation of each attached nitroxide label with respect to the polymer main chain and an isotropic distribution of these preferred orientations in the macroscopic sample due to the random distribution of polymer orientations. The ordering potential is expressed as a function of the angles θ and φ of the director in the rotational diffusion axis frame ($\mathbf{x}_R$, $\mathbf{y}_R$, $\mathbf{z}_R$), which is fixed relative to the magnetic frame ($\mathbf{x}_M$, $\mathbf{y}_M$, $\mathbf{z}_M$), which is in turn fixed relative to the structure of the nitroxide: $\mathbf{x}_M$ is the unit vector along the N−O bond direction, and $\mathbf{z}_M$ is along the unit vector along the axis of the nitrogen p-orbital. The relative orientations of the diffusion and magnetic axes are specified by the diffusion tilt angles $\Omega_D = (\alpha_D, \beta_D, \gamma_D)$, which are the Euler angles of the magnetic axes in the diffusion frame as defined in Figure 7, Chapter 3 in ref 24. The θ and φ are the polar and azimuthal angles, respectively, that define the orientation of the effective axis of internal rotation relative to the director expressed in the principal axes of nitroxide rotational diffusion tensor. The potential is given by the equation

$$-U(\theta,\varphi)/kT = \sum_{0<L,K\le 4,\text{even}} c_{LK}\left\{D^L_{0,K}(\theta,\varphi) + D^L_{0,-K}(\theta,\varphi)\right\} \quad (1)$$

where the c_{LK} terms refer to the strength and shape of the ordering potential and $D^L_{0,K}(\theta,\varphi)$ are the elements of the Wigner rotation matrix. When the c_{LK} terms are zero, the model becomes the simple Brownian rotational diffusion.

The rotational diffusion of nitroxide spin-labels attached to polymer chain segments has been approximated by superposition of the isotropic rotational diffusion of the polymer chain segment with the rotational diffusion coefficient, R_S, and by the internal rotation of the spin-label with the rotational diffusion coefficient, R_I.[25] When the nitroxide spin-label is attached to a polymer chain via a short tether, we can assume that $R_{prp} = R_S$ and $R_{pll} = R_I + R_S$. Here, the R_{pll} and R_{prp} are the parallel and perpendicular rotational diffusion coefficients, respectively. The number of parameters and the symmetry of the rotational components used in the simulations are along the lines described in ref 24b.

Differential Scanning Calorimetry (DSC). Thermal analysis was carried out using the Q10 differential scanning calorimeter manufactured by TA Instruments and calibrated with an indium standard. Cooling was accomplished by a TA Instruments quench cooler accessory. The DSC cell was purged with dry nitrogen flowing at a rate of 50 mL/min. Measurements were carried out in the range 163−383 K at a heating rate of 10 K/min.

X-ray Diffraction (XRD). X-Ray diffraction data were acquired on a Scintag X2 diffractometer using Cu Kα radiation generated at 45 kV and 40 mA and configured in a Bragg-Bretano focusing geometry. The scattering angle (2θ) was scanned at 0.03°/s in the range 3°−30° using a step size of 0.03°. The Bragg equation was applied to calculate the spacing, d, of Somasif platelets.

Fourier Transform Infrared (FTIR). Infrared spectra were recorded at room temperature using a Nicolet IMPACT400D FTIR spectrometer in the range 4000−400 cm^{-1} with 2 cm^{-1} resolution. Samples were prepared by grinding the powders with KBr in an agate mortar and pestle to a uniform consistency and pressed into a tablet.

Thermal Gravimetric Analysis (TGA). Weight loss measurements during controlled heating were carried out with TA Instruments Hi-Res TGA2950 and used to determine the amounts of residual water and polymer. Samples weighed typically ≈10 mg, and measurements were conducted during heating to 823 at 10 K min^{-1} under flowing air.

Results

XRD Measurements. Results for Somasif, NANO82, NANO96, and COMP99.8 measured in the 2θ range 3°−10° at ambient temperature are shown in Figure 1A. Somasif has two peaks, at $2\theta = 7.2°$ ($d_{001} = 1.23$ nm) and 9.3° (0.95 nm), indicating hydrated and dehydrated phases, respectively.[19,26] Peaks for NANO96 and NANO82 appear at $2\theta = 6.8$ ($d = 1.28$ nm) and 4.9 (1.78 nm). The increase of d in these samples is attributed to the intercalation of PEO into clay galleries: The galleries in which PEO is intercalated are 0.33 nm in NANO96 (1.28−0.95) and 0.83 nm in NANO82 (1.78−0.95). A weak diffraction peak at $2\theta = 9.3°$ for NANO82 (dotted arrow in Figure 1A) indicates the presence of a small amount of anhydrous Somasif. For COMP99.8, no peak shift from the original diffractions of neat Somasif was detected, indicating no PEO intercalation in the clay galleries. Compared to neat Somasif, the height of the peak at $2\theta = 9.3°$ from dehydrated layers is higher than that for $2\theta = 7.2°$ in the COMP99.8 because of the difference in hydration.

The XRD profile of NANO82 in the 2θ range 3°−30° (Figure 1B) exhibits several higher-order (00l) diffractions; peaks from anhydrous layers are marked with asterisks. Usually, PEO crystallites show strong peaks at about 19° and 24°.[27] The peak at 24° is a combination of the (112) and (032) reflections, and the peak at 19° corresponds to the (120) reflection. The NANO82 samples did not show these strong peaks.

DSC Measurements. DSC traces of PEO4k, NANO96, NANO82, and COMP99.8 are shown in Figure 2. No transitions were detected for NANO96, NANO82, and COMP99.8, while a distinct melting transition was observed for PEO4k at 338 K. The degree of crystallinity in PEO4k is calculated at 91%, using 222.2 J/g as the fusion enthalpy of PEO crystallites.[28]

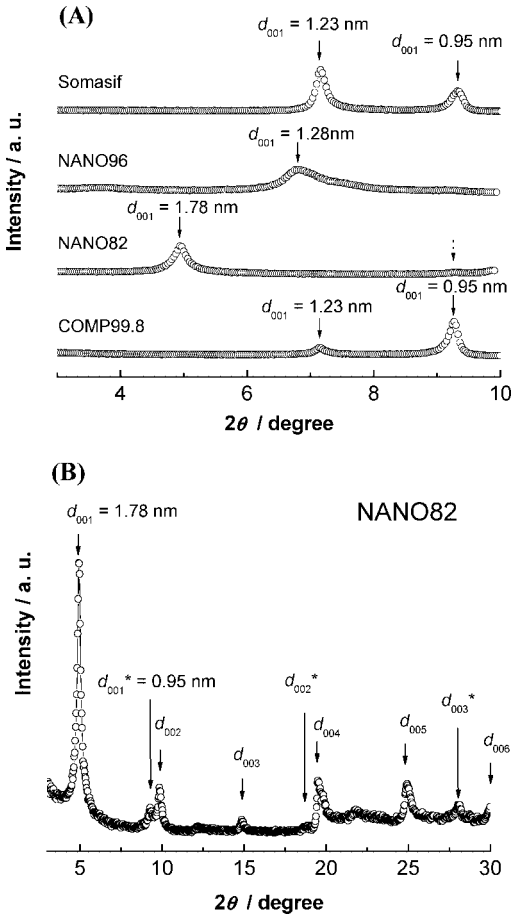

Figure 1. (A) XRD patterns of PEO4k, NANO96, NANO82, and COMP99.8 in the 2θ range 3°−10°. (B) XRD pattern of NANO82 in a wide 2θ range, 3°−30°.

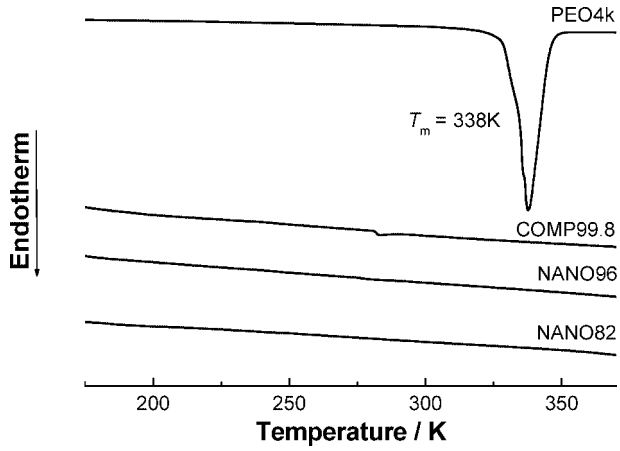

Figure 2. DSC traces for PEO4k, NANO96, NANO82, and COMP99.8.

FTIR Measurements. FTIR spectra of the PEO4k, NANO96, and NANO82 in the region 1500−1150 cm^{-1} are shown in Figure 3. In NANO96 and NANO82 samples, the strong adsorption at 1175−975 cm^{-1} associated with the Si−O stretching motion in the silicate was subtracted using the spectrum of neat Somasif.[3] For NANO96 and NANO82, only one component, at 1351 and 1355 cm^{-1}, respectively, was observed. Hoffmann and Rabolt reported that the bands at 1360 and 1343 cm^{-1} in crystalline PEO are associated with the CH_2 wagging motion,[29] while Li and Hsu observed only a single peak at 1349 cm^{-1} in molten PEO,[30] suggesting that the PEO chains in NANO96 and NANO82 were similarly amorphous.

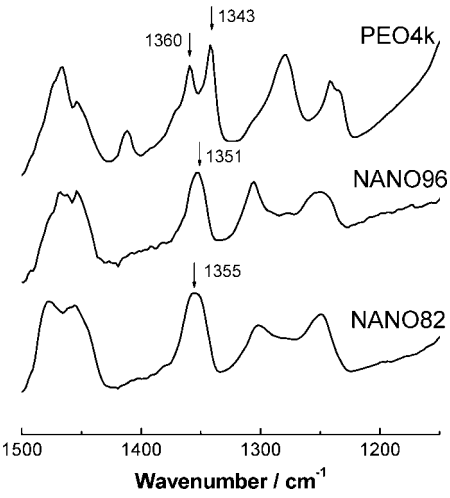

Figure 3. FTIR spectra of PEO4k, NANO96, and NANO82. The spectrum of Somasif was subtracted from the original spectra of NANO96 and NANO82; the subtracted spectra are shown.

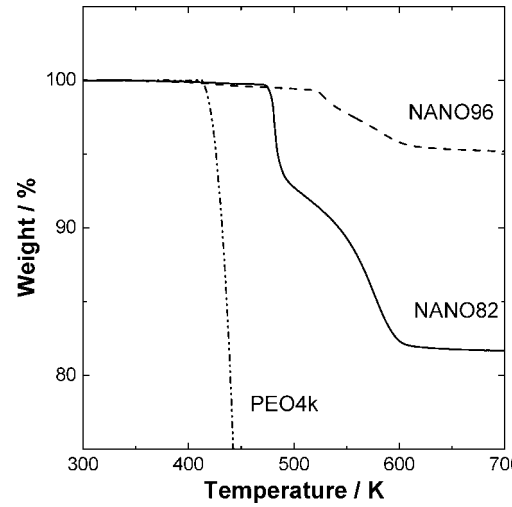

Figure 4. TGA curves of PEO4k, NANO82, and NANO96 measured in air.

TGA Measurements. Weight loss data for PEO4k, NANO96, and NANO82 are shown in Figure 4. The NANO96 and NANO82 samples showed higher decomposition temperatures than PEO4k, most likely because the diffusion of oxygen molecules is inhibited in the clay galleries: this is additional evidence for the intercalation of PEO. Moreover, the decomposition temperature of NANO96 is higher than that of NANO82, indicating the slower oxygen diffusion in the narrower galleries.

ESR Measurements. Selected experimental and simulated ESR spectra of PEO4k, NANO96, NANO82, and COMP99.8 in the range 100−410 K are shown in Figure 5. The temperature dependence of the ESR line shape is due to changes in the rotational rate of the nitroxide radical with correlation time, τ_c, defined as $1/(6(R_{prp}{}^2R_{pll})^{1/3})$.

The rigid-limit spectra observed at 100 K were successfully fitted using the NLSL program with very slow isotropic Brownian rotational diffusion of the spin-label ($R_{pll} = R_{prp} = 1 \times 10^3\ s^{-1}$). Best fits required a superposition of Lorentzian line shapes with Gaussian inhomogeneous broadening. The Gaussian line width is considered to reflect local interactions sensed by the nitroxide labels. The Gaussian line widths (ΔH) and the A and g tensors used for the best fits are listed in Table 2. The A_{zz} values were estimated from experimental spectra, and their

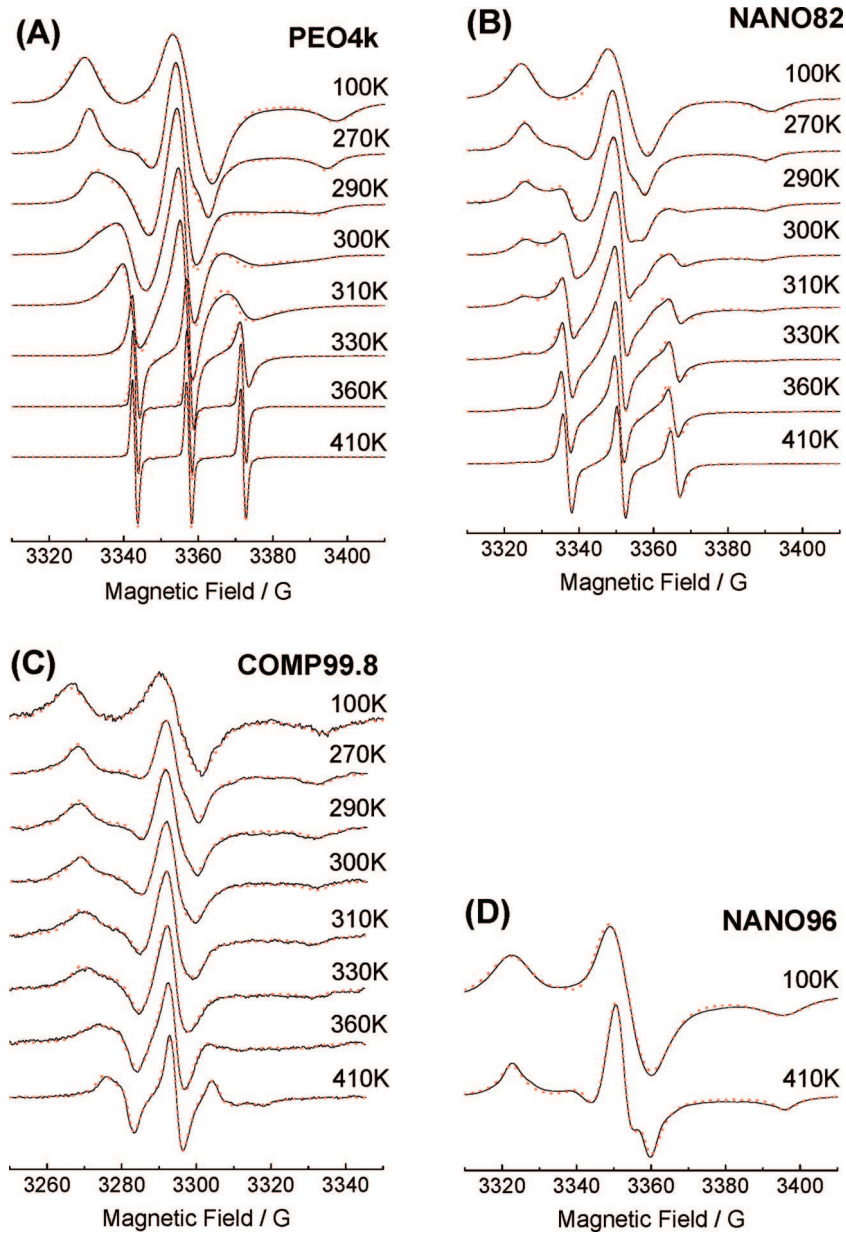

Figure 5. Temperature variation of ESR spectra (experimental spectra: full black lines; simulated spectra: red dotted lines) for PEO4k (A), NANO82 (B), COMP99.8 (C), and NANO96 (D).

Table 2. Parameters Used for the Simulation of ESR Spectra at 100 K

sample	g_{xx}	g_{yy}	g_{zz}	A_{xx}/G	A_{yy}/G	A_{zz}/G	ΔH/G
PEO4k	2.0088	2.0068	2.0025	5.7	4.0	33.6	7.3
NANO96	2.0084	2.0052	2.0021	7.7	4.3	36.8	8.0
NANO82	2.0088	2.0067	2.0026	5.9	4.2	33.4	7.4
COMP99.8	2.0090	2.0070	2.0028	5.7	4.0	33.9	7.4

accuracies are ±0.1 G for the PEO4k, NANO82, and NANO96 and ±0.5 G in COMP99.8 because of the lower S/N ratio.

The parameters R_S and R_I and the other parameters describing the local dynamics in PEO chains were determined by fitting experimental spectra, and the results are shown in Figure 5. ESR spectra of all samples were simulated with a single spectral component, with the exception of NANO82: Two distinct spectral components, fast and slow, were necessary to fit spectra for this sample. Arrhenius plots of R_S and R_I (rotational diffusion coefficient for the polymer segment and the spin-label, respectively) are shown in Figure 6A,B, and the corresponding activation energies E_S and E_I are listed in Table 3. The ordering potential coefficients c_{20} and c_{22} used to simulate experimental spectra are shown as a function of temperature in Figure 7A,B. For PEO4k, NANO82, and COMP99.8, the tilt angles β_D are almost constant (52 ± 5°), while the fitted value of β_D for NANO96 is significantly smaller, 11° at 410 K.

The percentage of the fast component in the NANO82 (Figure 8) is constant below 250 K, but above 250 K it rises suddenly and continues to increase with increasing temperature.

The effect of the dynamic parameters on the simulated line shapes was investigated in detail. In the Supporting Information, the variation of the parameters R_{prp}, R_{pll}, β_D, c_{20}, and c_{22} is shown and compared to the best-fitting simulated spectrum. The line shapes were very sensitive to the dynamic parameters for the PEO4k, NANO82, and COMP99.8, indicating the narrow range of the parameters that characterize the dynamics in these systems. On the other hand, the line shape for NANO96 was relatively insensitive to the dynamic parameters; this result is not surprising, as the nitroxide label in this system is near the rigid limit even at 410 K and the corresponding dynamic parameters cannot be determined accurately by X-band ESR.

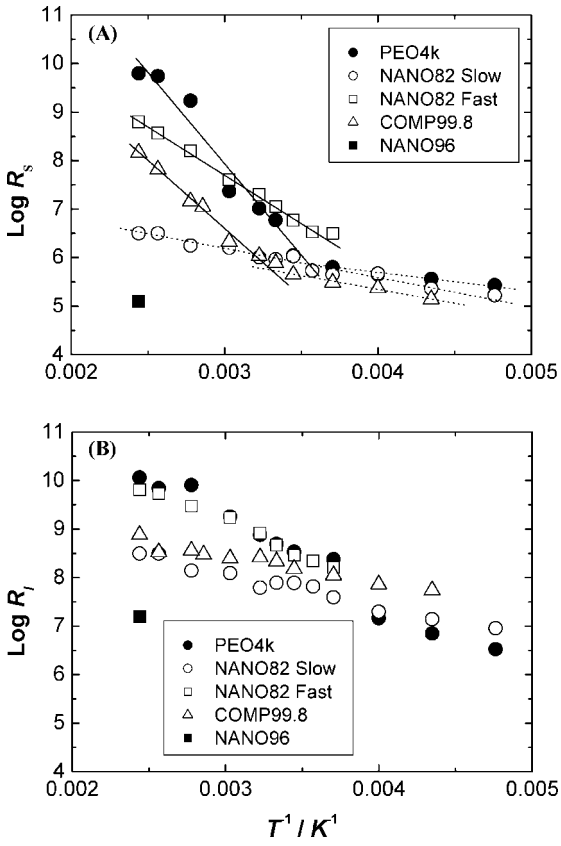

Figure 6. Arrhenius plots of the rotational diffusion coefficients R_S (A) and R_I (B).

Table 3. Activation Energies

sample	E_S (kJ/mol)	E_I (kJ/mol)
PEO4k	69,[a] 8[b]	32
NANO82 (slow component)	11	13
NANO82 (fast component)	37	26
COMP99.8	54,[c] 11[d]	9

[a] $T^{-1} < 0.0035$. [b] $T^{-1} > 0.004$. [c] $T^{-1} < 0.003$. [d] $T^{-1} > 0.0037$.

Discussion

Amorphous Structure of PEO in Nanocomposites. The XRD, FTIR, and DSC results shown in Figures 1–3 indicate the absence of crystalline PEO in the clay galleries. Moreover, the XRD results (Figure 1) show that PEO chains in NANO96 and NANO82 are intercalated in galleries with widths ≈0.33 and 0.83 nm, respectively. In such narrow galleries, the crystallization of PEO chains is inhibited, and no melting transition is detected by DSC (Figure 2). The IR peaks at 1351 cm^{-1} in NANO96 and 1355 cm^{-1} in NANO82 strongly suggest that PEO is amorphous (Figure 3).[30] Furthermore, NANO82 showed no diffraction peaks from PEO crystallites in Figure 1B. Taken together, these results lead to the conclusion that the PEO chains intercalated in the Somasif galleries are amorphous. PEO, present in COMP99.8 at very low concentration, is expected to be amorphous because of the adsorption onto Somasif platelets.

The absence of the glass transition in the data shown in Figure 2 is assigned to two factors. First, the glass transition of intercalated PEO may be very broad and not seen as a distinct step in the DSC trace. Second, the glass transition may be inhibited because of the lack of dynamic cooperativity of PEO segments.[31,32] It is reasonable to assume that the reduced cooperative motion in NANO82 and NANO96 is a result of PEO confinement in narrow galleries, <1 nm wide. This conclusion is in agreement with observations from intercalated

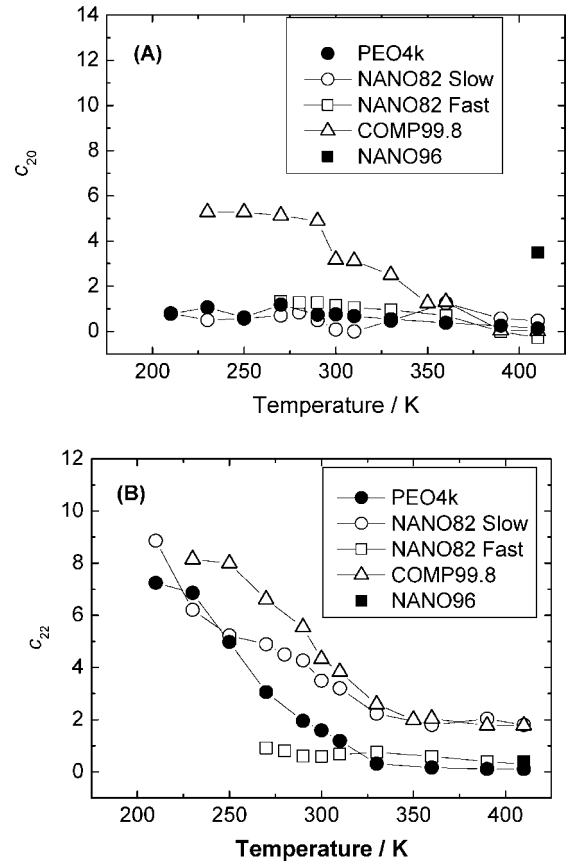

Figure 7. Temperature variation of the ordering potential coefficients, c_{20} and c_{22}.

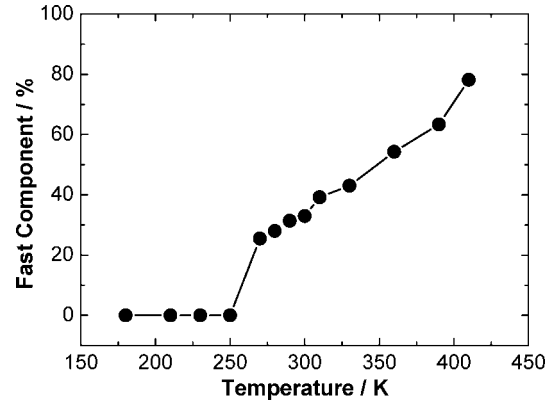

Figure 8. Temperature variation of the relative intensity (%) of the fast spectral component in NANO82.

PEO/montmorillonite (MMT) nanocomposites,[5–8] where no T_g and T_m were observed by DSC. TSC reveals a low motional activation energy, and solid-state ^2H NMR spectra show an averaging at a lower temperature compared to bulk PEO, but a rigid-limit spectral component even at high temperatures.

As described below, the parameters deduced from the simulation of the ESR spectra as a function of temperature allowed us to present a quantitative description of the rigid limit and averaged components, in terms of their correlation times and intensity ratio.

Local Environment of PEO in Somasif Galleries. ESR spectra at 100 K reflect the local environment around the spin-labels because their motion is frozen.[33] It is well-known that the A_{zz} value is sensitive to, and increases with, the local polarity,[33,34] as reported for nitroxide labels located near charged

Somasif platelets.[17–19] For NANO96, $A_{zz} = 36.8$ G, a value significantly larger than that of PEO4k, 33.6 G (Table 2). In the narrow 0.33 nm gallery of NANO96, a single PEO chain is tightly packed because the thickness of a PEO chain containing only trans bonds is about 0.37 nm, while the length of the monomeric unit $-C_2H_2O-$ is 0.35 nm.[10] The large A_{zz} of the NANO96 is due to the tight chain confinement between the charged Somasif platelets.

For NANO82, $A_{zz} = 33.4$ G, a value close to that of PEO4k (33.6 G), suggesting a lower local polarity in the larger 0.83 nm gallery. In addition to the electrostatic interaction with the clay, an additional factor that can decrease A_{zz} is the decrease in the PEO segmental density around the nitroxides because the polymer is polar. Results from both experimental and numerical studies have shown a decrease in the density of PEO intercalated into 0.8 nm galleries.[4,11] Experimentally, Wu and Lerner determined the density of PEO intercalated in montmorillonite (MMT) to be 0.8 g/cm^3, while that of bulk amorphous PEO is 1.1 g/cm^3.[4] Hackett et al. calculated the segmental density of PEO chains intercalated in the MMT using molecular dynamics and showed that the average segmental density of PEO in the galleries is also lower than that of bulk PEO.[11] We propose that the surprising lack of enhancement of A_{zz} in NANO 82 by electrostatic interaction with the silicate surface is caused by the competing effect of the reduced PEO segmental density in the gallery.

For COMP99.8, $A_{zz} = 33.9$ G, which is only marginally larger than for PEO4k and much smaller than that of NANO96. This result indicates that although the PEO chains are not intercalated in the clay, they are adsorbed on the charged silicate surface, and similarly to NANO82, the expected increase in the A_{zz} value due to contact with the charged surface is canceled by the decrease in the A_{zz} value due to the low PEO segmental density around the labels.

ESR spectra of NANO82 showed a superposition of two spectral components; the relative weight of the fast component increased with increase in temperature and was ≈80% at 410 K (Figure 8). The slow component clearly represents PEO segments interacting with the solid surface, leading to both a high A_{zz} and a low mobility. The accelerated dynamics of the fast component represents both the weaker interactions with the polar clay surface and a lower PEO segmental density. This conclusion is in accord with computer simulations, which showed the coexistence of fast and slow segmental relaxations and determined a higher segmental density with a slower segmental relaxation near the inorganic areas.[11,13,35] At higher temperatures the number of cations coordinated to the PEO oxygens decreases, leading to the increase of the relative intensity of the fast spectral component.

Assignment of Relaxation Modes Detected by Spin-Labeling. The Arrhenius plot of R_S, the rotational diffusion coefficient of PEO segments, shows a break around 280 K (Figure 6), and the activation energies, E_S, above and below the break point are 69 and 8 kJ/mol, respectively (Table 3). For relaxation phenomena in polymers such as the glass transition, the activation energy typically decreases at temperatures beyond the transition. Therefore, the increase of E_S with increasing temperature indicates that the nitroxide labels are mainly activated by different relaxation modes of the host polymer above and below the break point. These values can be compared with the activation energies, E_a, of relaxation modes in bulk PEO measured by dielectric spectroscopy, which have been studied in detail by Jin et al.[36] Bulk PEO shows four relaxation processes, α, β, γ, and γ'. The α relaxation is a local process associated with the crystalline phase. The β process originates in cooperative segmental motions in portions of the noncrystalline component. The γ process is assigned to local twisting of the main chains in both crystalline and noncrystalline regions. The γ' relaxation is attributed to the motion of PEO segments in the transition regions between the lamellae and the disordered interlamellar amorphous segments. The E_S value in the low-temperature region (8 kJ/mol) is comparable to the E_a of the γ-relaxation process (15 kJ/mol), indicating that the nitroxide labels are activated mainly by the local relaxation mode of PEO associated with γ relaxation in the low-temperature region. On the other hand, E_S above the break temperature, 69 kJ/mol, is in good agreement with the E_a of $\beta + \gamma + \gamma'$ relaxation (54 kJ/mol). In bulk PEO, β, γ, and γ' relaxations overlap above about 243 K,[36] and the cooperative segmental motion of the PEO main chain is detected by spin-labels only *above* the break temperature.

One may wonder why the spin-labels are not activated by the β relaxation in the low-temperature region. X-band ESR line shapes are not sensitive to dynamics with a correlation time, τ_c, outside the range of $10^{-11}-10^{-7}$ s.[17] As a result, the cooperative segmental motion is too slow to be detected by X-band ESR in the low-temperature region. Therefore, the ESR line shapes reflect only the local motions in the low-temperature region, the γ relaxation. However, as the cooperative segmental motional rate increases with an increase in the temperature and its τ_c becomes less than ca. 10^{-7} s, the cooperative segmental motion becomes detectable by X-band ESR. Therefore, the nitroxide label motion is activated by both the segmental motion and the local motions in the high-temperature region; the agreement between E_S and E_a of the $\beta + \gamma + \gamma'$ relaxation model strongly supports this conclusion.

Spatial Restriction of PEO Chain Mobility in Clay Galleries. The R_S values deduced from simulations of the ESR line shapes of the spin-label in the various samples are excellent indicators of the effect of the local environment. NANO96 has a very low log R_S value, 5.1, even at 410 K, compared to 9.8 for PEO4k (Figure 6A). The corresponding value for COMP99.8 at 410 K, 8.2, is slightly lower compared to that of PEO4k because of the adsorption of PEO chains onto the Somasif surface, but not much lower because of the low segmental density of the polymer. The latter result can also explain the lower E_S of the COMP99.8, 54 kJ/mol, compared to PEO4k, 69 kJ/mol (Table 3).

Figure 6 also indicates that the fast component in NANO82 has a higher mobility than PEO in COMP99.8. The release from the attraction of the silicate walls leads to a higher mobility even though the PEO chains are confined in the narrow galleries. From the A_{zz} value, the segmental density is estimated to be low in the galleries. In fact, E_S of the fast component is lower than that of the PEO4k (Table 3). The cooperative segmental region generally grows with a decrease in temperature.[37] The increase of the size of the cooperative segmental region is however suppressed and negligible in the gallery. Therefore, the fast relaxing component in the NANO82 retains a high mobility even at relatively low temperatures. As shown in Figure 6A, the R_S value of the fast component in NANO82 is higher than for PEO4k for $T^{-1} > 0.0032$.

Ordering Potentials. Best fits of ESR spectra were achieved with the ordering potential parameters c_{20} and c_{22}, which describe the shape of the ordering potential at a given temperature.[24] For PEO4k, c_{22} is sensitive to the temperature and much larger than c_{20} (Figure 7); above ca. 330 K, both c_{20} and c_{22} values become close to zero, indicating the random rotational diffusion of the labels. In this temperature regime the label motion is activated by the segmental motion of the PEO. We note that in this study the chain end of the PEO was labeled. The motion of the chain end is expected to be more isotropic than the inner segments. Therefore, the motional ordering of the labels becomes almost isotropic as the label motion is

activated by the segmental motion of the PEO main chain. The ordering potential parameters for NANO82 shows a similar tendency with that of the PEO4k: the behavior of the local motion around the label in NANO82 is similar to that in bulk PEO.

NANO96 showed very strong motional ordering even at 410 K, because of the low segmental mobility of the PEO, with large c_{20} and small c_{22} values at 410 K. The c_{20} coefficient leads to a maximum in the director orientation distribution along the $\mathbf{z}_R$ axis. Moreover, β_D (the angle between the internal rotation axis and $\mathbf{z}_M$) in NANO96 is quite small (11°) compared to those of the other samples (ca. 52°). In NANO96, the PEO chains are compressed in the extremely narrow galleries, and the conformation around the nitroxide is most likely distorted. Marek et al. showed that the conformation around the nitroxide label affected both the β_D value and the ordering potential parameters.[38]

In COMP99.8, both c_{20} and c_{22} have relatively high values in the low-temperature range. The combination of positive c_{20} and c_{22} values results in a maximum in the director orientation distributed to the $\mathbf{x}_R-\mathbf{z}_R$ plane.[24] The internal rotation of the label in COMP99.8 is essentially free compared to that in the PEO4k because of the excess free space and the isolation from interchain interactions and entanglements at the surface and leads to the unique ordering potential observed. A systematic study of the ordering potential of isolated polymer chains may give useful insight into the effect of interchain interactions on polymer chain dynamics.

Conclusions

The structure and mobility of PEO chains intercalated in layered silicates were compared with those of the bulk polymer. XRD, DSC, and FTIR measurements revealed that the crystallization of the intercalated PEO was inhibited due to the confinement in the narrow clay galleries.

The dynamic properties of PEO were estimated from the simulation of the temperature-dependent ESR spectra based on the MOMD model. In NANO96, the PEO chains were strongly compressed by the charged silicate platelets, and the polymer mobility was extremely low even at high temperature. The decrease in the PEO segmental density in the gallery was reflected in the spectra and the parameters used for simulation in NANO82. In this sample, fast- and slow-motional components were observed in the ESR spectra, and the ratio of the fast-motional component increased with an increase in temperature. The fast and slow relaxing components were attributed respectively to segments removed from and interacting with the solid walls in the gallery. The mobility of the fast-motional component in NANO82 was higher than that of the PEO chains in the COMP99.8, reflecting the reduced activation energy, even when compared to bulk PEO4k. It is clear from this study that the low segmental density and reduced dynamic cooperativities with neighboring segments determine the appearance of the fast segmental component with low activation energy in galleries of width 0.83 nm.

Acknowledgment. This study was supported by the Polymers Program of the National Science Foundation. The authors thank CO-OP Chemical, Japan, for the gift of Somasif ME-100 and are grateful to Professor D. E. Budil for his kind guidance on MOMD simulations. The authors also thank Dr. K. Yamamoto for his help with the TGA experiments and Dr. M. V. Motyakin for his help with experimental procedures and illuminating discussions.

Supporting Information Available: XRD data for NANO96 prepared via the melt intercalation method (Figure S-1); effect of parameter variation on the simulated spectra of PEO4k, NANO82, and COMP99.8 at 310 K and of NANO96 at 410 K (Figures S-2 to S-5, respectively). This material is available free of charge via the Internet at http://pubs.acs.org.

References and Notes

(1) Pinnavaia, T. J.; Beall, G. W. *Polymer-Clay Nanocomposites*; Wiley & Sons: London, 2000.
(2) Ajayan, P. M.; Schadler, L. S.; Braun, P. V. *Nanocomposite Science and Technology*; Wiley-VCH: Berlin, 2004.
(3) Aranda, P.; Ruiz-Hitzky, E. *Chem. Mater.* **1992**, *4*, 1395.
(4) Wu, J.; Lerner, M. M. *Chem. Mater.* **1993**, *5*, 835.
(5) Wong, S.; Vasudevan, S.; Vaia, R. A.; Giannelis, E. P.; Zax, D. B. *J. Am. Chem. Soc.* **1995**, *117*, 7568.
(6) Wong, S.; Vaia, R. A.; Giannelis, E. P.; Zax, D. B. *Solid State Ionics* **1996**, *86−88*, 547.
(7) Krishnamoorti, R.; Vaia, R. A.; Giannelis, E. P. *Chem. Mater.* **1996**, *8*, 1728.
(8) Vaia, R. A.; Sauer, B. B.; Tsu, O. K.; Giannelis, E. P. *J. Polym. Sci., Part B: Polym. Phys.* **1997**, *35*, 59.
(9) Harris, D. J.; Bonagamba, T. J.; Schmit-Rohr, K. *Macromolecules* **1999**, *32*, 6718.
(10) Bujdák, J.; Hackett, E.; Giannelis, E. P. *Chem. Mater.* **2000**, *12*, 2168.
(11) Hackett, E.; Manias, E.; Giannelis, E. P. *Chem. Mater.* **2000**, *12*, 2161.
(12) Chen, B.; Evans, J. R. G. *J. Phys. Chem. B* **2004**, *108*, 14986.
(13) Kuppa, V.; Menakanit, S.; Krishnamoorti, R.; Manias, E. *J. Polym. Sci., Part B: Polym. Phys.* **2003**, *41*, 3285.
(14) Elmahdy, M. M.; Chrissopoulou, K.; Afratis, A.; Floudas, G.; Anastasiadis, S. H. *Macromolecules* **2006**, *39*, 5170.
(15) Chrissopoulou, K.; Afratis, A.; Anastasiadis, S. H.; Elmahdy, M. M.; Floudas, G.; Frick, B. *Eur. Phys. J.* **2007**, *141*, 267.
(16) Anastasiadis, S. H.; Karatasos, K.; Vlachos, E.; Giannelis, E. P. *Phys. Rev. Lett.* **2000**, *84*, 915.
(17) Brik, M. E.; Titman, J. J.; Bayle, J. P.; Judeinstein, P. *J. Polym. Sci., Part B: Polym. Phys.* **1996**, *34*, 2533.
(18) (a) Jeschke, G.; Panek, G.; Schleidt, S.; Jonas, U. *Polym. Eng. Sci.* **2004**, *44*, 1112. (b) Panek, G.; Schleidt, S.; Mao, Q.; Wolkenhauer, M.; Spiess, H. W.; Jeschke, G. *Macromolecules* **2006**, *39*, 2191.
(19) (a) Miwa, Y.; Drews, A. R.; Schlick, S. *Macromolecules* **2006**, *39*, 3304. (b) Miwa, Y.; Drews, A. R.; Schlick, S. *Polym. Prepr. (Am. Chem. Soc., Div. Polym. Chem.)* **2006**, *47*, 839.
(20) Finnigan, B.; Jack, K.; Campbell, K.; Halley, P.; Truss, R.; Casey, P.; Cookson, D.; King, S.; Martin, D. *Macromolecules* **2005**, *38*, 7386.
(21) Törmälä, P.; Lindlberg, L. *Polymer* **1973**, *14*, 481.
(22) Schneider, D. J.; Freed, J. H. In *Biological Magnetic Resonance*; Berliner, L. J., Reuben, J., Eds.; Plenum: New York, 1989; Vol. *8*, Chapter 1, pp 1−76.
(23) Budil, D. E.; Lee, S.; Saxena, S.; Freed, J. H. *J. Magn. Reson. A* **1996**, *120*, 155.
(24) (a) Meirovitch, E.; Nayeem, A.; Freed, J. H. *J. Phys. Chem.* **1984**, *88*, 3454. (b) Xu, D.; Budil, D. E.; Ober, C. K.; Freed, J. H. *J. Phys. Chem.* **1996**, *100*, 15867. (c) Liang, Z.; Freed, J. H. *J. Phys. Chem. B* **1999**, *103*, 6384. (d) Earle, K. A.; Budil, D. E. In *Advanced ESR Methods in Polymer Research*; Schlick, S., Ed.; Wiley: Hoboken, NJ, 2006; Chapter 3, pp 53−83.
(25) Pilar, J. In Schlick, S., Ed.; *Advanced ESR Methods in Polymer Research*; Wiley: Hoboken, NJ, 2006; Chapter 6, pp 133−163, and references therein.
(26) Maiti, P. *Langmuir* **2003**, *19*, 5502.
(27) Fraisse, F.; Morlat-Thérias, S.; Gardette, J.-L.; Nedelec, J.-M.; Baba, M. *J. Phys. Chem. B* **2006**, *110*, 14678.
(28) Braun, W.; Hellwege, K.-H.; Knappe, W. *Kolloid Z. Z. Polym.* **1967**, *215*, 10.
(29) Hoffmann, C. L.; Rabolt, J. F. *Macromolecules* **1996**, *29*, 2547.
(30) Li, X.; Hsu, S. L. *J. Polym. Sci., Polym. Phys. Ed.* **1984**, *22*, 1331.
(31) Donth, E. *J. Non-Cryst. Solids* **1982**, *53*, 325.
(32) Jackson, C. L.; McKenna, G. B. *J. Non-Cryst. Solids* **1991**, *131*, 221.
(33) Griffith, O. H.; Jost, P. C. In Berliner, L. J., Ed.; *Spin Labeling Theory and Applications*; Academic Press: New York, 1976; p 453.
(34) Griffith, O. H.; Dehlinger, P. J.; Van, S. P. *J. Membr. Biol.* **1974**, *15*, 159.
(35) Kuppa, V.; Manias, E. *J. Chem. Phys.* **2003**, *18*, 3421.
(36) Jin, X.; Zhang, S.; Runt, J. *Polymer* **2002**, *43*, 6247.
(37) Adam, G.; Gibbs, J. H. *J. Chem. Phys.* **1965**, *43*, 139.
(38) Marek, A.; Czernek, J.; Steinhart, J.; Labsky, J.; Stepanek, P.; Pilar, J. *J. Phys. Chem. B* **2004**, *108*, 9482.

MA800214Q